ICES REPORT 10-02

February 2010

Modeling of Bone Conduction of Sound in the Human Head Using hp Finite Elements I. Code Design and Verification

by

L. Demkowicz, P. Gatto, J. Kurtz, M. Paszynski, W. Rachowicz,
E. Bleszynski, M. Bleszynski, M. Hamilton, and C. Champlin

The Institute for Computational Engineering and Sciences
The University of Texas at Austin
Austin, Texas 78712

MODELING OF BONE CONDUCTION OF SOUND IN THE HUMAN HEAD USING hp FINITE ELEMENTS I. CODE DESIGN AND VERIFICATION

L. Demkowicz[a], P. Gatto[a], J. Kurtz[a], M. Paszyński[b], W. Rachowicz[c], E. Bleszyński[d], M. Bleszyński[d], M. Hamilton[e], C. Champlin[f]

[a] Institute for Computational Engineering and Sciences, University of Texas at Austin
[b] AGH University of Science and Technology, Cracow, Poland
[c] Cracow University of Technology, Cracow, Poland
[d] Monopole Research
[e] Dept. of Mechanical Engineering, University of Texas at Austin
[f] College of Communications, University of Texas at Austin

1. Introduction

Motivation

Hearing impairment remains the primary disability among military personnel. Sound pressure levels caused by proximity to aircraft engines or impulse noise from large caliber weapons may easily exceed the pain threshold value of 100 dB.

The focus of this project is to to develop a reliable numerical model for investigating the bone-conducted sound in the human head. The problem is difficult because of a lack of fundamental knowledge regarding the transmission of acoustic energy through non-airborne pathways to the cochlea. A fully coupled model based on the acoustic/elastic interaction problem with a detailed resolution of the cochlea region and its interface with the skull and the air pathways, should provide an insight into this fundamental, long standing research problem.

The project builds on an interaction of experts in numerical wave propagation – Drs. Elisabeth and Marek Bleszynski from Monopole Research with a team at the University of Texas headed by Dr. Leszek Demkowicz and including two experts on wave propagation and hearing science: Dr. Mark Hamilton and Dr. Greg Champlin.

Literature review

Bone-conducted sound.. The fact that vibration of the skull causes a hearing sensation has been known since the 19th century. This mode of hearing was termed hearing by bone conduction. Al-

though there has been more than a century of research on hearing by bone conduction, its physiology is not completely understood. For and early account of the phenomenon as cause of partial deafness see [8]. Further summaries of those early works can be found in Hood (J. Acoust. SOC. Am., 34: 1325-1332, 1962) and Naunton (Chapter I in Modern Development in Audiology, J. Jerger, ed., Academic Press, New York, 1963). Lately, new insights into the physiology of hearing by bone conduction have been reported. Knowledge of the physiology, clinical aspects, and limitations of bone conduction sound is important for clinicians dealing with hearing loss. Factors contributing to bone conduction of sound, such as inertia of the middle ear ossicles and of the cochlear fluids, and sound radiated into the external ear canal have been investigated by S. Stenfelt and R. Goode in [19]. The effects of bone conduction of sound were studied via a finite element model by F. Böhnke F, and W. Arnold in [7]. This study showed the influence of bone conduction on pressure signals at the cochlea wall. The first simultaneous sound pressure measurements in scala vestibuli and scala tympani of the cochlea in human cadaveric temporal bones were presented by E. Olson et al. in [14]. Finally, among other fundamental works done by E. Olson on bone conduction of sound and its interplay with the cochlea we want to recall [15] and [6].

Coupled (visco)-elasticity with acoustics.. The variational formulation for the coupled elasticity/acoustics problem utilized in this project is classical and has been extensively studied over the last two decades, see e.g. [9]. The term *weak coupling* has different meanings. The involved variables: elastic displacement $\boldsymbol{u}$ and acoustic pressure p are not forced to match each other on the elastic/acoustic interface. Instead, the variational formulation incorporates additional off-diagonal flux terms representing the interaction in between the two fields and resulting from the interface conditions. It is essential that either field represents a dual quantity for the other. Hence the term "weak" contrary to "strong" couplings where two variables match each other at both continuous and discrete levels along the interface. A second meaning of the term "weak coupling" refers to the fact that the coupling terms represent compact perturbations of the terms on the main diagonal corresponding to elasticity and acoustics. This guarantees automatically that the Galerkin discretization of the problem will be *asymptotically stable*.

***hp**-elements..* The presented work builds on FE technology of hp-adaptive finite elements, see [2, 4] and the literature therein. Motivated with our 2D experience [5] and the needs of this project, we have started to build a new version of our hp3D code for multiphysics applications and coupled problems.

Overview of the paper.

We begin with Section 2 describing the specifics of the governing coupled problem and numerical challenges. Section 3 provides an short overview on geometrical modeling and our FE technology. For project of this complexity, code verification is a critical issue, and we report on our verification tests in Section 4. Section 5 describes in detail a geometry model used for this project

and offers sample numerical results illustrating the possibilities of the presented technology. Final comments and plan of future work presented in Section 6 conclude the presentation.

2. The Head Problem

In this section we review shortly specifics of the head problem. The problem falls into the category of general coupled elasticity/acoustics problems discussed in Appendix AppendixA with a few minor modifications. The domain Ω in which the problem is defined is the interior of a ball including a model of the human head, and it is split into an acoustic part Ω_a, and an elastic part Ω_e. Depending upon a particular example we shall study, the acoustic part Ω_a includes:

- air surrounding the human head, bounded by the head surface and a truncating sphere; this part of the domain may include portions of air ducts leading to the middle ear through mouth and nose openings;
- cochlea,
- an additional layer of air bounded by the truncating sphere and the outer sphere terminating the computational domain, where the equations of acoustics are replaced with the corresponding *Perfectly Matched Layer* (PML) modification.

The elastic part of the domain includes:

- skull,
- tissue.

By the term *tissue* we understand here all parts of the head that are not occupied by the skull (bone) and the cochlea. This includes the thin layer of the skin and the entire interior of the head with the brain. We will assume that the elastic constants for the whole tissue domain are the same. As the viscosity constant for the tissue is four orders of magnitude smaller than that for the skull, an alternative approach would be to model the tissue as an acoustical fluid, neglecting the shear waves in the brain.

The acoustic wave is represented as the sum of an incident wave p^{inc} and a scattered wave p. Only the scattered wave is assumed to satisfy the radiation (Sommerfeld) condition,

$$\frac{\partial p}{\partial r} + ikp \in L^2(\mathbb{R}^3) \tag{2.1}$$

The different types of boundaries discussed in Appendix AppendixA reduce only to the interface between the elastic and acoustic subdomains, and the outer Dirichlet boundary for the acoustic domain. Material interfaces between the skull and tissue, as well between the air and the PML air do not require any special treatment.

The final formulation of the problem has the form A.11, with the bilinear and linear forms defined as follows.

$$\begin{aligned} b_{ee}(\boldsymbol{u},\boldsymbol{v}) &= \int_{\Omega_e} \left(E_{ijkl}u_{k,l}v_{i,j} - \rho_s\omega^2 u_i v_i\right)\, d\boldsymbol{x} \\ b_{ae}(p,\boldsymbol{v}) &= \int_{\Gamma_I} pv_n\, dS \\ b_{ea}(\boldsymbol{u},q) &= -\omega^2\rho_f \int_{\Gamma_I} u_n q\, dS \\ b_{aa}(p,q) &= \int_{\Omega_a} \left(\boldsymbol{\nabla} p\boldsymbol{\nabla} q - k^2 pq\right)\, d\boldsymbol{x} \\ l_e(\boldsymbol{v}) &= -\int_{\Gamma_I} p^{inc} v_n\, dS \\ l_a(q) &= -\int_{\Gamma_I} \frac{\partial p^{inc}}{\partial n} q\, dS \end{aligned} \tag{2.2}$$

A symmetric formulation is enabled by dividing the equations of acoustics with factor $\rho_f\omega^2$,

$$\begin{aligned} b_{ee}(\boldsymbol{u},\boldsymbol{v}) &= \int_{\Omega_e} \left(E_{ijkl}u_{k,l}v_{i,j} - \rho_s\omega^2 u_i v_i\right)\, d\boldsymbol{x} \\ b_{ae}(p,\boldsymbol{v}) &= \int_{\Gamma_I} pv_n\, dS \\ b_{ea}(\boldsymbol{u},q) &= -\int_{\Gamma_I} u_n q\, dS \\ b_{aa}(p,q) &= \tfrac{1}{\omega^2\rho_f} \int_{\Omega_a} \left(\boldsymbol{\nabla} p\boldsymbol{\nabla} q - k^2 pq\right)\, d\boldsymbol{x} \\ l_e(\boldsymbol{v}) &= -\int_{\Gamma_I} p^{inc} v_n\, dS \\ l_a(q) &= -\tfrac{1}{\omega^2\rho_f} \int_{\Gamma_I} \frac{\partial p^{inc}}{\partial n} q\, dS \end{aligned} \tag{2.3}$$

Notice that we refer to the outer normal unit vector $\boldsymbol{n}$ always *locally*, i.e. in the formula for the coupling bilinear form b_{ae} involving elasticity test functions $\boldsymbol{v}$, versor $\boldsymbol{n}$ points outside of the elastic domain, whereas in the formula for the coupling bilinear form b_{ea} involving acoustic test functions q, versor $\boldsymbol{n}$ points outside of the acoustic domain. The normal components v_n and u_n present in the coupling terms are thus opposite to each other, and the formulation is indeed symmetric.

2.1. Non-dimensionalization. Material and temporar scales

The material data are summarized in Table 1. For elastic materials, the speed of compressional waves and shear waves is given by the formulas.

$$c_p^2 = \frac{E(1-\nu)}{(1+\nu)(1-2\nu)\rho}, \quad c_s^2 = \frac{E}{2(1+\nu)\rho} \tag{2.4}$$

This is a purely mechanical problem and we can choose three independent units for for setting up a non-dimensional version of the equations:

material	E[MPa]	ν	ρ[kg/m^3	c_p[m/s]	c_s[m/s]
tissue (brain)	0.67	0.48	1040	75	15
skull (bone)	6500	0.22	1412	2293	1374
cochlea (water)			1000	1500	
air			1.2	344	

Table 1: Material constants and speed of sound for compressional and shear waves.

Reference length h_0 represents length of a tetrahedron in the geometry model necessary to resolve geometrical details. We choose $h_0 = 1$[cm] $= 10^{-2}$[m]. Parameter h_0 should not be confused with the finite element length which varies accordingly to wave number regime and order of approximation. The choice of reference length implies that geometry data for the head problem (non-dimensional nodal coordinates) will be of order 1-10.

Reference angular velocity: $\omega_{ref} = 2\pi \cdot 200$Hz[rad/s]. The reference angular velocity corresponds to the dominating frequency in the spectrum of the actual sound source.

Reference pressure: p_0. We choose $p_0 = 100$ [Pa], a value corresponding to the threshold of pain for the human ear in air.

We introduce now the following non-dimensional quantities:

Coordinates: $\hat{x}_i = \frac{x_i}{h_0}$,

Elastic displacements: $\hat{u}_i = \frac{u_i}{h_0}$

Angular frequency: $\hat{\omega} = \frac{\omega}{\omega_{ref}}$,

Incident pressure: $\hat{p}^{inc} = \frac{p^{inc}}{p_0}$,

Scattered pressure: $\hat{p} = \frac{p}{p_0}$,

Elastic module: (for both skull and tissue) $\hat{E} = \frac{E}{p_0}$,

Densities: (for skull, tissue, cochlea and air) $\hat{\rho} = \frac{\rho \omega_{ref}^2 h_0^2}{p_0}$,

Wave speeds: (for skull, tissue, cochlea and air:) $\hat{c} = \frac{c}{\omega_{ref} h_0}$.

The form of the equations remains identical with the original formulation, with the non-dimensional quantities replacing the original ones. As usual, we drop the "hats" in the notation.

2.2. Optimal scaling

The weak coupling offers the possibility of an additional scaling of elastic displacements. We set

$$\hat{u}_i = t\widehat{\hat{u}}_i$$

This is possible because there are no strong continuity conditions relating pressure and elastic displacements across the fluid/solid interfaces. Replacing u_i with tu_i in the variational formulation, we get

$$\begin{cases} tb_{ee}(\boldsymbol{u}, \boldsymbol{v}) + b_{ae}(p, \boldsymbol{v}) & = l_e(\boldsymbol{v}) \qquad \forall \boldsymbol{v} \\ tb_{ea}(\boldsymbol{u}, q) + b_{aa}(p, q) & = l_a(q) \qquad \forall q \end{cases}$$

o To preserve the symmetry of the formulation, we divide the second equation by the scaling factor to obtain the final form of the equations.

$$\begin{cases} tb_{ee}(\boldsymbol{u}, \boldsymbol{v}) + b_{ae}(p, \boldsymbol{v}) & = l_e(\boldsymbol{v}) \qquad \forall \boldsymbol{v} \\ b_{ea}(\boldsymbol{u}, q) + \frac{1}{t} b_{aa}(p, q) & = \frac{1}{t} l_a(q) \qquad \forall q \end{cases}$$

In order to improve the conditioning and minimize the round-off effects, we choose the scaling parameter in such a way that, after the scaling, the stiffness terms in elasticity (for the skull) and acoustics (air) are of the same order, i.e.

$$tE = \frac{1}{t\rho_f \omega^2} \quad \Rightarrow \quad t = \frac{1}{\sqrt{E\rho_f}\omega}$$

Notice that as a byproduct of the optimal scaling, the rescaled elastic displacement is expected to be of order one. Indeed, with the new stiffness terms being of the same order, the rescaled elastic displacements and pressure should be of the same order. As the intensity of the scattered pressure is expected to be of order of incident pressure, the non-dimensional scattered pressure should be of order one and, therefore, the same should hold for the rescaled elastic displacements.

2.3. PML modification

In the PML part of the acoustical domain, the bilinear form b_{aa} is modified as follows:

$$b_{aa}(p, q) = \int_{\Omega_{a,PML}} \left(\frac{z^2}{z' r^2} \frac{\partial p}{\partial r} \frac{\partial q}{\partial r} + \frac{z'}{r^2} \frac{\partial p}{\partial \psi} \frac{\partial q}{\partial \psi} + \frac{z'}{r^2 \sin^2 \psi} \frac{\partial p}{\partial \theta} \frac{\partial q}{\partial \theta} \right) r^2 \sin \psi dr d\psi d\theta \qquad (2.5)$$

Here r, ψ, θ denote the standard spherical coordinates and $z = z(r)$ is the PML stretching factor defined as follows,

$$z(r) = (1 - \frac{i}{k} \left[\frac{r-a}{b-a} \right]^{\alpha}) r \qquad (2.6)$$

Here a is the radius of the truncating sphere, b is the external radius of the computational domain ($b - a$ is thus the thickness of the PML layer), i denotes the imaginary unit, k is the acoustical wave

number, and r is the radial coordinate. In computations, all derivatives with respect to spherical coordinates are expressed in terms of the standard derivatives with respect to Cartesian coordinates. In all reported computations, parameter $\alpha = 6$. For a detailed discussion on derivation of PML modifications and effects of higher order discretizations see [13, 4].

3. Overview of the FE Technology

3.1. Geometry Modeling

Mesh Based Geometry Description.. Geometry modeling is the foundation of any FE code. The presented technology builds on the concept of the *Mesh Based Geometry (MBG)* description, discussed extensively in e.g. [2, 4]. The object of interest is partitioned into a mesh-like structure consisting of blocks of the same shapes as those used for finite elements: prisms, hexas, tets and pyramids for 3D problems, and quads and triangles for 2D applications. Each of the blocks comes with a parametrization, i.e. a map $\boldsymbol{x}_b(\boldsymbol{\eta})$ mapping a corresponding *reference block* onto the particular block within the physical domain. These parametrizations must be at least C^0- compatible. Intuitively speaking, if the reference prisms, hexas, tets and pyramids are covered with uniform meshes and identical number of partitions (elements) along the edges, the geometry maps will map those uniform meshes onto a regular FE mesh in the physical domain. This is precisely the concept behind the classical *algebraic mesh generators*.

There are two fundamental technical difficulties in constructing a MBG description for an object. The first one deals with partitioning of the object into blocks and setting appropriate connectivities - the task encountered in any unstructured mesh generation. For academic geometries consisting just of few blocks, this can be done "by hand", by preparing an appropriate input file. For more complicated geometries, we write separate short programs that prepare the input files, see [21] for non-trivial examples. But for most practical problems, we have to resort to third party mesh generators like NETGEN [16] that we have used in this project.

The second technical task deals with the construction of compatible parametrizations. The main idea here is to employ a *bottom-up* approach used e.g. in unstructured mesh generation. Besides the geometrical blocks, we introduce geometrical entities of lower dimension: *points (vertices), (segments of) curves, and quads and triangles*. Having defined the points, we define first (parametrizations for) the curves connectining the points. Next, we construct parametrizations for quadrilateral and triangular faces in such a way that they match the already defined parametrizations for edges. Mathematically speaking, given a quad or triangle, the task is to *extend* parametrization of its edges to the interior of the figure. This is done using techniques of *transfinite interpolation* and *implicit parametrizations*. For C^0-conforming parametrizations, the task is relatively easy; if we demand more global regularity, these constructions become quite technical (see e.g. [3]). Finally, having constructed the parametrizations for faces, we use again the transfinite parametrization techniques to extend them to the whole blocks.

Interfacing with NETGEN.. To describe geometries involved in this project, we have interfaced with Joachim Schoeberl's NETGEN [16]. NETGEN takes on input a *Constructive Solid Geometry* (CSG) description of the geometrical object. Given a number of *primitives* like half-space, interior or exterior of a sphere, cylinder or cone, etc., we use Boolean operations to define the object. NETGEN identifies then the resulting 2D polygonal interfaces, 1D edges and vertices, and uses *Delaunay* and *Advancing Front* mesh generation techniques to generate a mesh consisting of linear tetrahedra. The mesh generation is done using the bottom-up approach. First, nodes are placed at CSG vertices, then 1D meshes are generated along the CSG edges, followed by generation of triangular meshes on interfaces and, finally, generation of tetrahedral meshes inside of the resulting 3D polyhedral domains. NETGEN generates meshes with a minimum number of tetrahedra implied by geometrical scales. This fits perfectly the philosophy of MBG description.

Extruding membranes and adding prismatic layers.. An attempt to mesh thin-walled structures like membranes present in this project, with tetrahedral meshes leads to a prohibitive number of elements and distorted tets. To avoid the problem, the membranes are first identified as 2D interfaces, forcing NETGEN to generate meshes conforming to the membranes and only then extruded into thin 3D objects. More precisely, defining a membrane involves setting up the surface occupied by the membrane, a set of surfaces bounding the actual membrane, and an additional set of surfaces bounding the extrusion domain. The simplest example is provided by extruding a membrane inside of a cylindrical shell, see Fig. **??**. The membrane is first identified with a plane cutting through the cylinder. The inner cylinder bounds the actual extruded 3D membrane, while the outer cylinder terminates the set of extruded triangles. All vertex points in the interior of the 2D membrane are extruded into line segments, whereas the points on the outer cylinder stay unduplicated. All triangles within the inner cylinder are extruded into prisms. Triangles within the cylinder wall may be extruded into prisms, tets or pyramids, depending upon the number of triangle vertices located on the outer cylindrical surface.

In this way, the extrusion process has forced us to introduce into the code both prisms and pyramids. The prisms are also the element of choice for discretizing problems with spherical geometry (used for code verification in this project) and implementation of *Perfectly Matched Layer*. In both cases, we start with a triangular mesh on a sphere and extrude it in the radial direction into a number of layers of prismatic elements.

Upgrading to curvilinear geometry.. Generation of geometrical models used in this project is done within a separate *Geometrical Modeling Package* (GMP) and consists of the following steps.

Step 1: Prepare an input file defining involved surfaces (planes, spheres, cylinders and cones).

Step 2: Use the surfaces and CSG description to prepare input for NETGEN. Generate the mesh.

Step 3: Read into GMP information on the mesh generated by NETGEN: a list of vertex coordinates, tets to vertex connectivities and, triangles to vertex connectivities, for all triangles located on surfaces input into NETGEN. Along with the connectivities, NETGEN returns also the corresponding subdomain number (for tets) or surface number (for triangles). The routine interfacing with NETGEN generates then automatically the remaining GMP objects for the linear geometry: e dges (curves, straight line segments at this point) and remaining triangles (within the interior of subdomains) along with curve to point, and triangle to point connectivities.

Step 4: Extrude membranes and additional prism layers.

Step 5: Complete the connectivities: blocks to triangles and quads, blocks to curves, triangles and quads to curves. The connectivities include also information on *orientations*.

Step 6: Use the information on surfaces defined in Step 1 and transfinite interpolation techniques to upgrade the model to fully curvilinear tets, prisms and pyramids conforming to the predefined surfaces.

Step 7: Verify shape regularity checking for negative jacobians.

The information about surfaces and the complete info on connectivities are necessary for the transfinite interpolation, see [10] for details.

Despite every attempt to automate the process of model generation, we have not managed to eliminate the human interface. Input of data into NETGEN is done manually. Two general purpose routines extrude membranes and add additional layers of prismatic elements. Upgrading, however, the extruded blocks to curvilinear geometries involves providing an additional information which we have not managed to automate and which requires a user provided geometry customization routine.

The final step in defining the geometry includes checking for negative jacobians done at a set of discrete points corresponding to a uniform mesh in the reference domain with 10 segments per GMP curve.

3.2. Finite Element Discretization

Design assumptions. Multiphysics and weak couplings.. The project has been done using a new 3D hp code being developed at ICES. More precisely, this very project has forced us to go back to the drawing board and build a new 3D hp code. Building on technology described in [4], we have made a number of assumptions extending significantly from our previous work.

Elements of all shapes. Supporting prisms, hexas, tets and pyramids in a single code forces an object oriented programming style. For instance, a single element routine serves elements of all shapes.

Multiphysics. The code supports all discretizations forming the exact sequence: H^1-, $\boldsymbol{H}(\mathbf{curl})$-, $\boldsymbol{H}(\mathrm{div})$-, and L^2-conforming elements. In this project, though, we use the continuous elements only. Different variables may be supported throughout the whole domains, or in specific subdomains only, like in the discussed project. An extra attribute - subdomain number, included in GMP data structure, is used to specify variables (elastic displacement, pressure) to be supported within the subdomain along with corresponding material data.

Weak couplings. Nodes on subdomain interfaces support variables for all adjacent subdomains. For this project, nodes on elastic/acoustic interface support both elastic displacement $\boldsymbol{u}$ and pressure p. This enables weak couplings through additional terms in the global stiffnes matrix like in this project.

Costrained approximation. The code supports 1-irregular meshes. Accounting for constrained nodes is done automatically and remains hidden from the user.

On top of the geometry definition, introducing a specific problem requires a number of user provided routines including a routine setting physical attributes (unknown fields to be supported) for each subdomains, order of approximation for the initial mesh elements and boundary conditions. The user has to provide also element routines computing element matrices for the specific problem. The logic of the code enables flexible definition of the multiphysics setting. For instance, the "brain" in this project may be modeled using elasticity or just acoustics. Changing the model requires modifying literally a single line in the routine setting up the definition of physics for the subdomains.

Initial mesh generation. Exact geometry and isoparametric elements.. Each GMP block corresponds to a single element in the initial FE mesh. Generation of finer meshes, including those corresponding to uniform h-refinements, is done through mesh refinements. The initial mesh generation has thus been reduced to a simple interface between the GMP and the hp3D code. All connectivities and orientations are copied from GMP into hp3D data structure. The only non-trivial operation is the generation of geometry d.o.f. which is done by performing Projection Based (PB) interpolation of the GMP maps for edges, faces and elements. The C^0-compatibility of the GMP parametrizations guarantees consistency of the resulting geometry d.o.f. The code supports the use of both *isoparametric* and *exact geometry* elements. The latter utilize directly the GMP maps and require the two codes be linked together. Both types of elements have their advantages and disadvantages. With the exact geometry elements, the geometry errors are eliminated, whereas the isoparametric elements reproduce global (linearized) rigid body modes (at the discrete level). For a detailed discussion on PB interpolation, exact geometry and isoparametric elements, see [2, 4].

Hierarchical shape functions.. One of the many challenges we had to face in this project was the construction of hierarchical spaces of shape functions for elements of all types, including the much neglected pyramid. In order to obtain an H^1 conforming FE space, such spaces must be constructed

in a way such the global basis functions are continuous across interlement faces and edges. In 2D and for hexas only meshes, compatibility of element shape functions on common faces and edges is enforced by the use of sign factors originally proposed by Szabo, see [20, 2, 4]. The use of sign factors is accounted for in the assembling procedure and complicates significantly implementation of constrained approximation (hanging nodes).

The situation is much more difficult for elements with triangular faces. The inherent conflict between hierarchical construction of shape functions and irrotational invariance may result in a situation when a single face shape function for an element must be connected with all shape functions for the neighboring element, even for regular meshes. One way to avoid the problem is to set up element coordinates in a proper way. For tets only meshes, Ainsworth and Coyle [1] have shown that one can solve the problem by considering tetrahedra of two types. Implementing the procedure requires resetting tets to vertex connectivities.

In the presented implementation we have followed a more radical way proposed originally by Ph. Devloo[1]. The edge and face basis functions are defined first on edges and faces using the edge and face parametrizations, and then extended into the neighboring elements. In other words, we first define the global basis functions and only then identify element shape functions as *restrictions* of the basis functions to the elements. This implies that the orientations (maps from local to global coordinates for edges and faces) are *accounted for in the shape functions routines*. One may think thus about not a single element but a family of elements for all possible variations of orientations. The input to element shape functions includes thus element type (prism, brick, tet, pyramid), order and orientation for element nodes and master element coordinates xi_i of a point within the element. The routine returns then the number of the element shape functions, their values and derivatives. For a detailed description of the element shape functions, see [10]. For alternative constructions see the work of Solin [], Zaglmair and Schoeberl [17] and, for pyramids, Nigam and Phillips [].

3.3. Parallel Multifrontal Direct Solver

Multi-physics problems usually generate huge linear systems of equations, which are not well conditioned, and thus, the applicability of iterative solvers is frequently limited. In addition, iterative solvers typically exhibit lack of robustness (indefinite problems, high-contrast materials, elongated elements, etc.). Moreover, iterative solvers may be slower than direct solvers when a system of equations with several right hand sides needs to be solved, as it occurs in this problem (multiple illumination directions). For these reasons we have decided to use a direct solver.

The large size of coupled multiphysics problems typically requires the use of *parallel* direct solvers. The current state-of-the-art are the *parallel multi-frontal* solvers, e.g. MUMPS solver (http://graal.ens-lyon.fr/MUMPS/). However, due to wide fronts (high p) of variable size (adaptiv-

[1] Private communication.

ity), a direct use of such solvers is rather limited.

The parallel multi-frontal solver, whose development has been partially motivated by this project, interfaces with the hp3D code utilizing the domain decomposition paradigm. The FE mesh is partitioned into multiple subdomains. Each sub-domain is associated with a single processor, possibly with multiple cores, allowing for the multi-thread execution. The solver utilizes a three level elimination tree. The bottom and the middle levels are generated for each subdomain separately, while the top level is created globally for all subdomains (processors). The bottom level builds upon the nodal trees created during the h refinements executed by the FE code. The middle level of the elimination tree is created by a graph partitioning algorithm, based on a graph representation of a single subdomain, consisting of multiple initial mesh elements. Finally, the top level of the elimination tree builds upon the partition of the computational mesh into multiple subdomains. At this point of code development, standard libraries like METIS are used to construct both the middle-level and the top level elimination trees.

The algorithm can be summarized in the following steps.

Step 1: A sequential frontal solver is executed in parallel for each sub-domain. The solver uses the bottom and the middle level elimination trees and computes partial LU factorizations to obtain the Schur complement of the subdomain internal degrees of freedom with respect to the interface degrees of freedom. The LU factorizations are stored at nodes of the elimination tree for a possible future reutilization.

Step 2: The global interface problem is solved. This is done by utilizing a mutli-level elimination pattern based on nested dissections algorithm and the global elimination tree. The subdomains Schur complements are joined into pairs, and fully assembled degrees of freedom are eliminated. New Schur complements corresponding to those degrees of freedom that haven't been eliminated yet, are computed. The step is repeated until a single interface problem is obtained. Every step of the elimination is executed using a parallel solver run on multiple processors, with the number of processors doubled in each step. The final interface problem is solved using all processors.

Step 3: Backsubstitution is executed in a reverse order utilizing LU decompositions obtained during the first two steps of the algorithm.

The key for an efficiency of the multi-frontal solver lies in a flexible numbering algorithm for local degrees of freedom at each node of the elimination tree. This is done by building on the nodal-based data structure of hp3D. Recall that by nodes we mean element vertices, edges, faces and interiors. Each node owns a variable number of d.o.f. corresponding to the node type, its order p, and the number of supported variables. Partially assembled stiffness matrices and their LU decompositions are stored using the concept of a hyper matrix. The hyper matrix consists of several

sub-matrices corresponding to FE nodes. The nodes keep links (in a hash table manner) to the corresponding matrices called the p-blocks. The degrees of freedom to be eliminated are identified by browsing nodes, following the links to the p-blocks and recognizing the p-blocks which have been fully assembled.

At this point of the code development, the sequential and parallel versions of the MUMPS solver are used in all discussed steps of the algorithm.

3.4. Graphical post-processing

The graphical output from the code is produced by an interface with the Visualization Toolkit (VTK) [18]. VTK is a freely available collection of C++ classes that enable the visualization of a wide variety of datasets. The present interface is based most directly on the class vtkUnstructuredGrid. In VTK, an unstructured grid is represented by an array of points with associated scalar or vector-valued data, and a collection of linear cells that connect the points to form, for example, tetrahedra, prisms, pyramids and hexahedra. Curvilinear geometry and higher order solutions are represented by introducing a user specified number of subdivisions on top of the existing finite element mesh. This abstract representation is then passed through a visualization pipeline that either renders an image on the screen or writes the output to an image file. The user is then able to interact with the dataset by for example, rotating the object, zooming in or out, clicking on individual elements to make them invisible, or "clipping" the entire dataset with a plane to see the solution in the interior. The interface also allows the user to generate an animation for the complex valued solution to a time-harmonic problem by generating a sequence of frames that display the quantity $\Re e^{i\omega t} p$ at discrete times t (here p is the complex pressure).

4. Code Verification

Code verification was one of the most tedious aspect we had to face in this project. We started with a simple case of an imploding spherical acoustic wave hitting a sphere composed of two elastic materials and comparing the numerical solution to the analytical solution. This was a rather primitive test since only eight tetrahedra – one per octant – and eight prisms approximate the elastic sphere, and there is no high contrast between the material constants. The second test dealing with a multilayered elastic sphere illuminated with a aplane way, was considerably more challenging. The FE solution was compared with the analytical Mie series solution in terms of Bessel and Hankel functions. The test was run for four possible scenarios with different material constants and different number of elements.

An Imploding Sphere Problem

The first verification test was performed by hitting the elastic sphere with an imploding spherical acoustic wave. An analytical solution of the elastic displacement $\mathbf{u}$ can be easily derived. We

postulate a spherically-symmetric solution of the form $u_i = x_i f(r)\cos\omega t$ which implies that

$$u_r = r f(r)\cos\omega t$$

After we introduce the displacement into the Navier-Stokes equations of elastodynamics

$$\mu u_{j,kk} + (\lambda+\mu)u_{k,kj} = \varrho\ddot{u}_j$$

we find a differential equation for f which has the non singular solution

$$f(r) = C\frac{kr\cos kr - \sin kr}{r^3}$$

where $k^2 = \varrho\omega^2/(2\mu+\lambda)$ and C is a constant. By means of Hook's law, the stress corresponding to $\mathbf{u}$ is:

$$\sigma_{rr} = 2\mu\frac{\partial u_r}{\partial r} + \lambda\left(\frac{2u_r}{r} + \frac{\partial u_r}{\partial r}\right). \tag{4.7}$$

Let's now consider the acoustic pressure p. If we assume a time-harmonic solution of the homogeneous wave equation, then $p = p(x_i)$ satisfies the Helmholtz equation of acoustics:

$$-\Delta p - k'^2 p = 0$$

where k' is the wavenumber. Again, if we assume a spherically-symmetric solutions we have

$$\left(\frac{\partial^2}{\partial r^2} + \frac{2}{r}\frac{\partial}{\partial r} + k'^2\right)p = 0$$

and after applying the substitution $p = f/r$ we obtain that f satisfies the simple equation

$$f'' + k'^2 f = 0$$

which implies that $f = Ae^{ik'r} + Be^{-ik'r}$ and $p = (Ae^{ik'r} + Be^{-ik'r})/r$. We may call the above two componets of p as the incident, p^{in}, and the scattered wave, p^{sc}, respectively.

One way to obtain the spherically-symmetric solution of coupled elastodynamics and acoustics is to assume the incident acoustic wave (parameter A), and evaluate the scattered acoustic wave (parameter B) and amplitude of vibrations in the solid (parameter C), so that adequate continuity conditions between solid and fluid are satisfied. Alternatively, we can prescribe the vibrations of the solid (by setting, for instance, $C = 1$), and find the incident and scattered acoustic waves (parameters A and B). We follow the second approach. Thus we assume the solution in the solid as:

$$u_r = \frac{k}{r}\cos kr - \frac{1}{r^2}\sin kr$$

The coupling conditions on the surface of the solid sphere, at $r = a$, satisfy:

$$\begin{aligned} \text{Continuity:} \quad & \frac{\partial p}{\partial r} = \omega^2\varrho_f u_r(a) \\ \text{Equilibrium:} \quad & \sigma_r(a) = -p(a) \end{aligned}$$

Expressing in the above condition for the stress σ_r by Eq. (4.7), and using definitions of u_r and total p we end up with 2 equations for the two unknown parameters A and B which specify the incident and scattered acoustic waves.

We performed this test on a sphere made of eight tetrahedra, one per octant, and eight prisms. The inner material was characterized by $\rho = 1$, $\mu = \lambda = 1$ was the outer material was characterized by $\rho = 1$, $\mu = \lambda = 0.25$. The total radius of the layered sphere was 1 and we solved the problem for $\omega = 1.1$ using sixth order elements. The profile of the real part of the radial displacement is shown in Figure (1). Since the mesh was so primitive it made little sense to compute convergence rates.

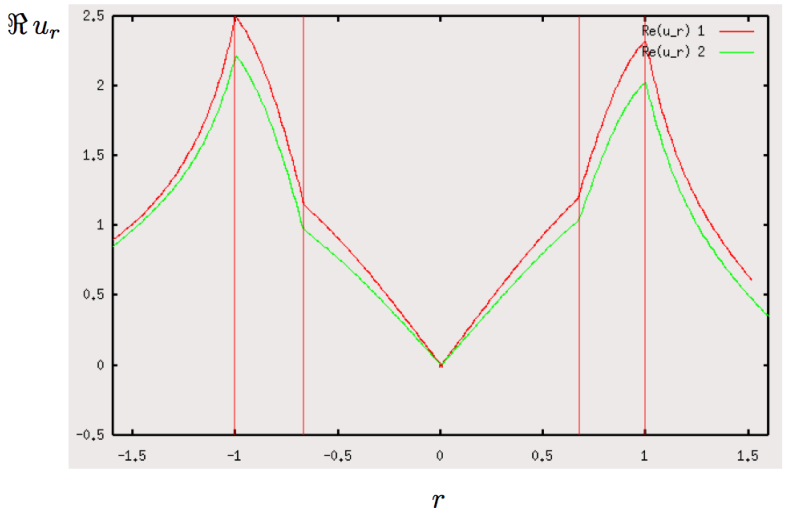

Figure 1: imploding sphere test. Green curve is the exact solution, the red curve is FEM solution for $p = 6$, and vertical red bars are interfaces between materials; elastic sphere has $r = 1$.

Multiple Spheres Problem

This verification builds on a comparison with an analytical solution for a general multiple spheres problem presented in [11]. The elastic sphere may be composed of an arbitrary number of spherically symmetric layers, each made of a different material. The sphere is iluminated with a plane acoustic wave propagating in the z-direction. The analytical solution is expressed in terms of Mie series of spherical Bessel and Hankel functions. The comparison is done by displaying both analytical and FE solutions (displacement, pressure) along the z-axis.

We considered the case of a sphere made of four spherical shells of different elastic materials. Four different scenarios were investigated:

(P1) low contrast material constants and many prismatic layers within each elastic spherical shell, see Table (2);

(P2) low contrast material constants and fewer prismatic layers within each elastic spherical shell, see Table (3);

(P3) high contrast material constants and many prismatic layers within each elastic spherical shell, see Table (4);

(P4) high contrast material constants and fewer prismatic layers within each elastic spherical shell, see Table (5).

Problems (P1) and (P3) are quite large - the number of d.o.f. ramps up to 5 million d.o.f for $p = 6$, while problems (P2) and (P4) are a bit smaller with 2.5 million d.o.f for $p = 6$. We were able to solve problem (P1) and (P3) with $p = 2, 3, 4$ and problem (P2) and (P4) with $p = 2, 3, 4, 5$ in the low frequency regime $\omega = 1.1$. For all four cases we have obtained a perfect matching with the analytical solution for all p's as it can be seen from Figures **??**, and 5.

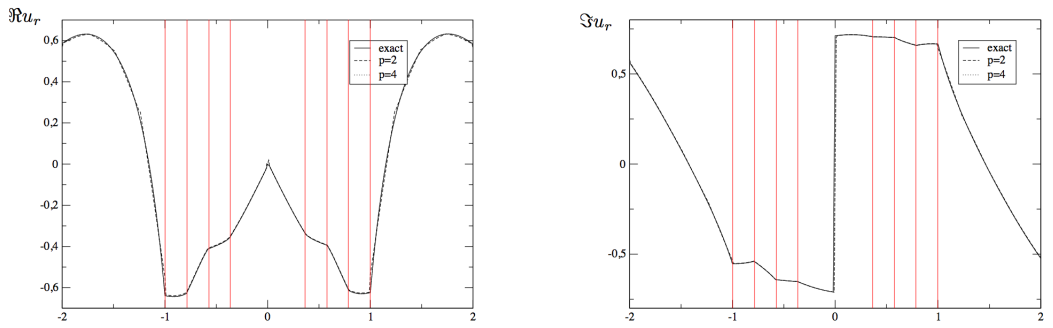

(a) real part of the radial displacement

(b) imaginary part of the radial displacement

Figure 2: problem (P1). Radial component of the elastic displacement; the vertical red lines represents the interfaces between the 4 materials.

5. Numerical Experiments

5.1. Geometry

Our simplified model of the head is constituted by 19288 elements: 16004 tetrahedra, 3228 prisms and 56 pyramids. As previously discussed, the pyramid is needed as a connecting element between a tetrahedron and a prism. The total number of nodes is 89961. The fully curvilinear geometry reconstructed by our code is shown in Figure 6. We solved the problem for 13 different

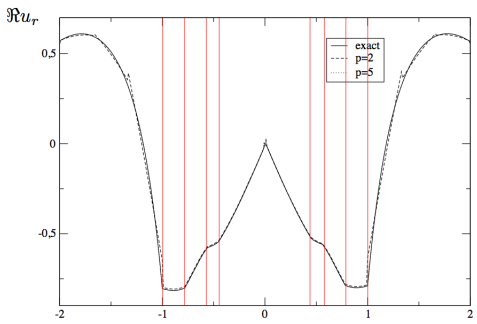

(a) real part of the radial displacement

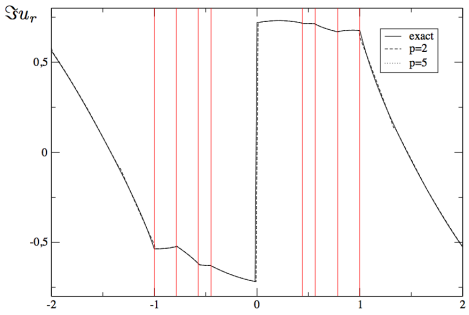

(b) imaginary part of the radial displacement

Figure 3: problem (P2). Radial component of the elastic displacement; the vertical red lines represents the interfaces between the 4 materials.

Shell	**Material**	**# of layers**	**Density**	**Young modulus, Poisson ration**				**Radius**
			ϱ	$\Re E$	$\Im E$	$\Re \nu$	$\Im \nu$	r
I	a	-	1.0	0.625	0.0	0.2	0.0	0.3
II	a	1	1.0	0.625	0.0	0.2	0.0	0.37
III	b	3	1.0	2.5	0.0	0.25	0.0	0.58
IV	c	3	0.3	0.5	0.0	0.2	0.0	0.79
V	d	3	2.0	5.0	0.0	0.3	0.0	1.0
VI	air	4						
VII	PML	2						

Table 2: problem (P1). Four ideal materials with material constants of same order of magnitude are considered.

incident directions of an acoustic plane wave; they correspond to increments of $\pi/12$ in the (x, y)-plane starting from $(0, -1, 0)$. We were able to solve the problem for $p = 2, 3, 4, 5$; in the case of $p = 5$ the system has 1070190 degrees of freedom.

5.2. Results

We computed the pressure of the lower and upper interface of the basilar membrane with the cochlea as a function of the incidence. The results as shown in Figure 7 and 8; notice that we are obtaining very good agreement for $p = 3, 4, 5$ for all incident directions. As seen from Figure 7(a) and 7(c) the results we obtained for $p = 2$ is totally off. We observed a similar behavior for the imaginary part of the pressure, hence the results for case $p = 2$ are not shown in Figure 8. A possible explanation of the poor results for $p = 2$ is that membranes lock for this order of approximation. This is one the many reason why the use of high order elements is essential for a successful study of the phenomenon.

Shell	Material	# of layers	Density	Young modulus, Poisson ration				Radius
			ϱ	$\Re\, E$	$\Im\, E$	$\Re\, \nu$	$\Im\, \nu$	r
I	a	-	1.0	0.625	0.0	0.2	0.0	0.45
II	b	1	1.0	2.5	0.0	0.25	0.0	0.56
III	c	2	0.3	0.5	0.0	0.2	0.0	0.78
IV	d	2	2.0	5.0	0.0	0.3	0.0	1.0
V	air	3						
VI	PML	2						

Table 3: problem (P2). Four ideal materials with material constants of same order of magnitude are considered.

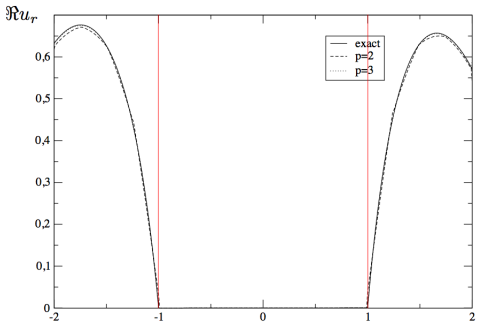

(a) real part of the radial displacement

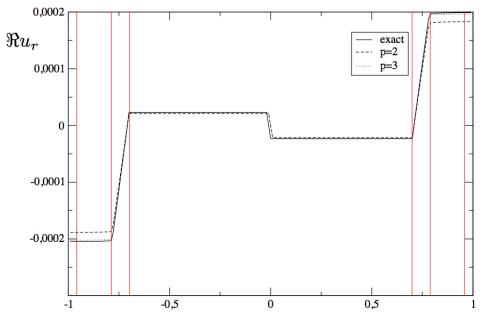

(b) real part of the radial displacement in the sphere

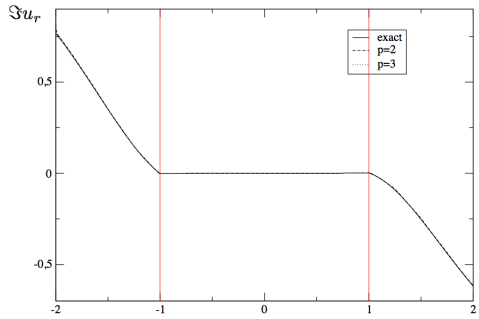

(c) imaginary part of the radial displacement

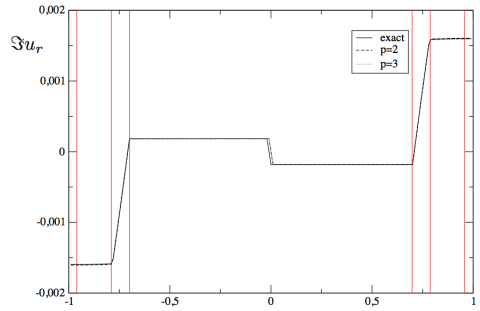

(d) imaginary part of the radial displacement in the sphere

Figure 4: Radial component of the elastic displacement; the vertical red lines represents the interfaces between the 4 materials.

6. Conclusions and Future Work

Geometry.. As mentioned in Section 3, we have not managed to fully automate the process of defining the geometry. To make it worse, our code still contains a "prayer component". NETGEN checks the shape regularity of generated tetrahedra but does it only for affine simplices. After the

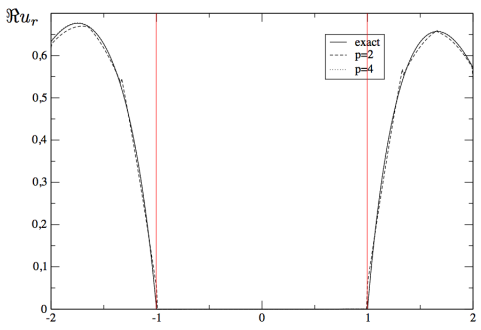

(a) real part of the radial displacement

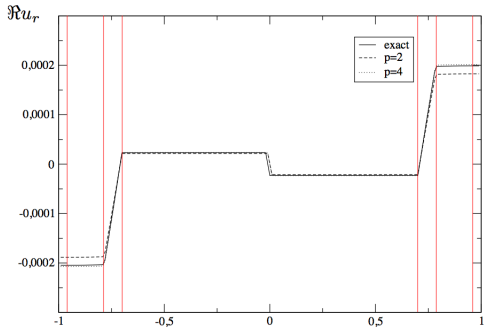

(b) real part of the radial displacement in the sphere

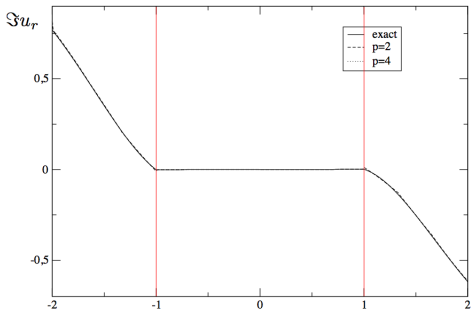

(c) imaginary part of the radial displacement

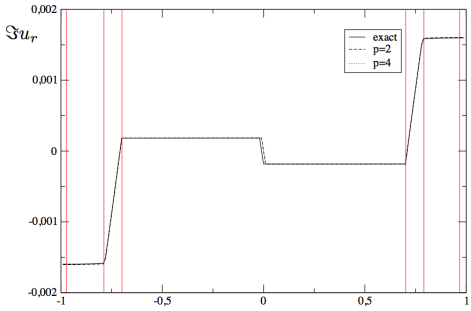

(d) imaginary part of the radial displacement in the sphere

Figure 5: Radial component of the elastic displacement; the vertical red lines represents the interfaces between the 4 materials.

Shell	**Material**	**# of layers**	**Density**	**Young modulus, Poisson ration**				**Radius**
			ϱ	$\Re\, E$	$\Im\, E$	$\Re\, \nu$	$\Im\, \nu$	r
I	tissue	-	835.4	29616.41	1.952	1.388 E-5	2.876 E-5	0.56
II	tissue	1	835.4	29616.41	1.952	1.388 E-5	2.876 E-5	0.7
III	skull	3	1.0	2.6	0.0	0.3	0.0	0.784
IV	cork	3	150.0	539.715	0.0	0.173	0.0	0.964
V	steel	3	6666.7	5964829.39	0.0	0.355	0.0	1.0
VI	air	4						
VII	PML	2						

Table 4: problem (P3). Four materials with material constants of different order of magnitude are considered.

upgrade to curvilinear geometry, we pray that the generated maps have no negative jacobians as we have no guarantee that this will not happen. Indeed, generating the model discussed in this paper took a couple of iterations with NETGEN. Quality assurance for the geometrical model generation should be done within the mesh generator and it requires a more tied interface between NETGEN

Shell	**Material**	**# of layers**	**Density**	**Young modulus, Poisson ration**				**Radius**
			ϱ	$\Re\, E$	$\Im\, E$	$\Re\, \nu$	$\Im\, \nu$	r
I	tissue	-	835.4	29616.41	1.952	1.388 E-5	2.876 E-5	0.7
II	skull	1	1.0	2.6	0.0	0.3	0.0	0.784
III	cork	2	150.0	539.715	0.0	0.173	0.0	0.964
IV	steel	2	6666.7	5964829.39	0.0	0.355	0.0	1.0
V	air	3						
VI	PML	2						

Table 5: problem (P4). Four materials with material constants of different order of magnitude are considered.

and GMP.

On the positive side, once the geometry has been defined, we can use it for multiple FE simulations involving different loads and material data, as the control of discretization error is done through local p- or h-refinements rather than multiple mesh regenerations.

hp *refinements..* Examples presented in this paper have been obtained using p-refined meshes only. The use of higher order elements is absolutely critical for succesful simulations of the discussed problem as the difference between the results obtained using quadratic and higher order elements indicates locking. This suggests starting with $p = 3$, at least for the thin-walled subdomains in the problem (membranes, skull). We have not experimented yet with (local) p-adaptivity.

We are in process of adding h-refinements to the code. This challenging extension of the code includes development of data structure algorithms for supporting the refinements and the constrained approximation package. The main challenge here are the complexity of the algorithms (code) and their efficiency. We pursue the idea of data structures and algorithms based on FE nodes [2, 4] but with some non-trivial modifications, and we hope to report soon on this part of the work.

Parallel solver.. Even the simplest verification examples reported in this paper, involve solution of systems of equations with many milion d.o.f. and large fronts resulting from the use of higher order elements. This necessitated the development of the parallel direct solver without which none of the more complicated examples could be solved. The solver, builds on the idea of the nodal trees borrowed from our hp3D data structures but it is being developed as an independent piece of software that could be interfaced with other FE codes.

Bone conduction study.. The actual parameter and sensitivity study on the presented problem using the described geometrical model, will be reported in a forthcoming second part of this paper. Our ultimate goal includes building a more complicated geometry model from MRI scans using geometry reconstruction techniques [3].

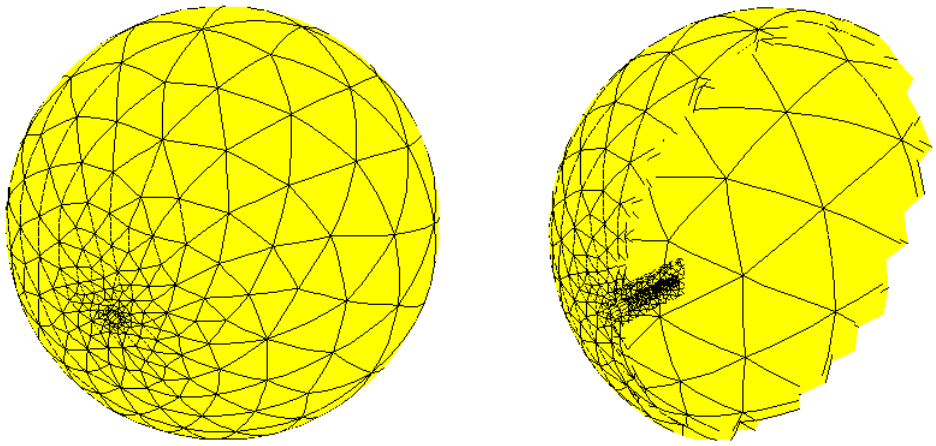

(a) skull (b) cross section of skull

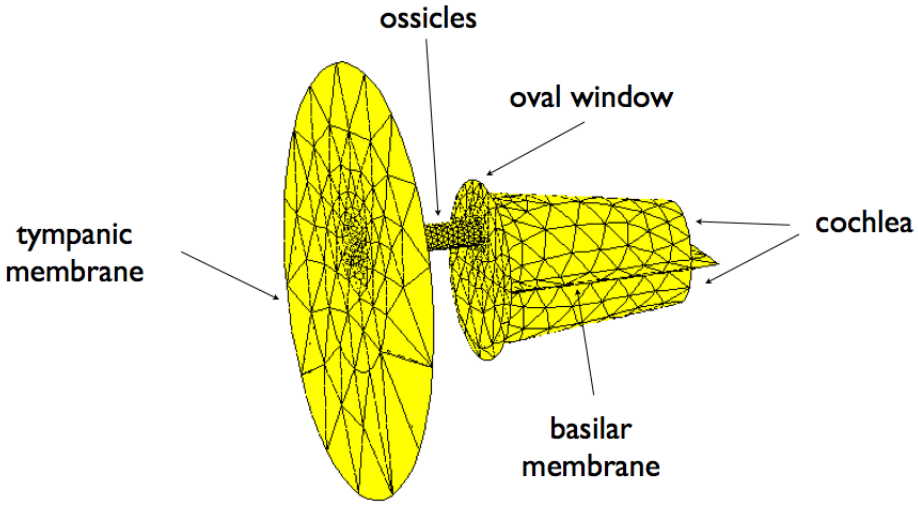

(c) middle ear

Figure 6: head model. Mesh has 19288 elements.

AppendixA. Formulation of the Coupled Elasticity/Acoustics Problem

In this opening section, we review the derivation of the variational formulations for acoustics, elasticity and then for the ultimate coupled elasticity/acoustics problem.

AppendixA.1. Linear Acoustics Equations

The classical linear acoustics equations are obtained by linearizing the isentropic form of the compressible Euler equations expressed in terms of density ρ and velocity vector v_i, around the

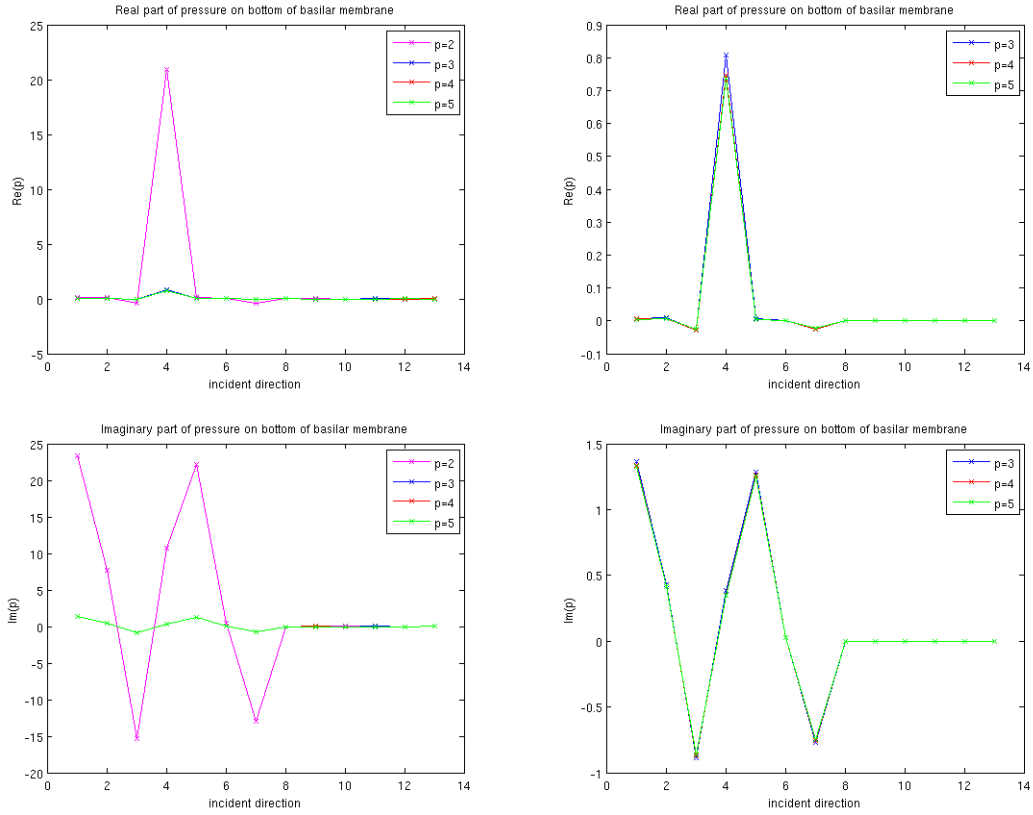

Figure 7: pressure on lower interface of basilar membrane.

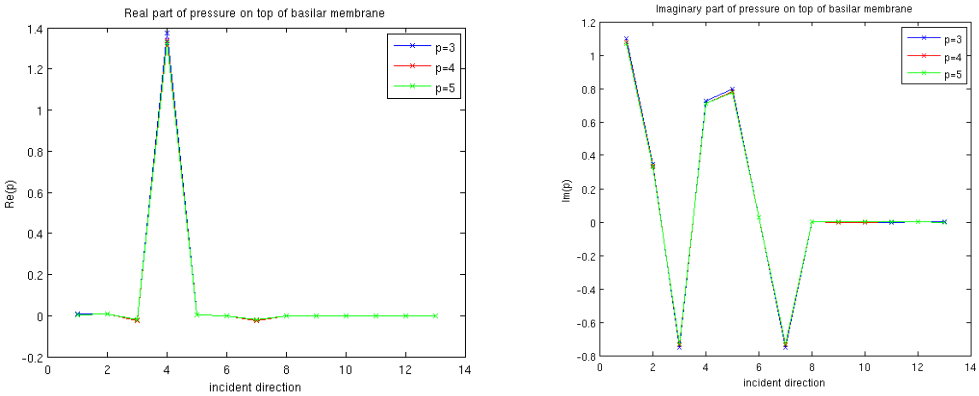

Figure 8: pressure on upper interface of basilar membrane.

hydrostatic equilibrium position $\rho = \rho_0, v_i = 0$. Perturbing the solution around the equilibrium position,

$$\rho = \rho_0 + \delta\rho, \quad v_i = 0 + \delta v_i,$$

and linearizing the Euler equations, see e.g. [12], we obtain a system of four first order equations in terms of unknown perturbations of density $\delta\rho$ and velocity δv_i,

$$\begin{cases} (\delta\rho)_{,t} + \rho_0(\delta v_j)_{,j} = 0 \\ \rho_0(\delta v_i)_{,t} + (\delta p)_{,i} = 0\,, \end{cases}$$

with δp denoting the perturbation in pressure. For the isentropic[2] flow, the pressure is simply an algebraic function of density,

$$p = p(\rho)$$

Linearization around the equilibrium position leads to the relation between the perturbation in density and the corresponding perturbation in pressure

$$p = \underbrace{p(\rho_0)}_{p_0} + \frac{dp}{d\rho}(\rho_0)\delta\rho$$

Here p_0 is the hydrostatic pressure, and the derivative $\frac{dp}{d\rho}(\rho_0)$ is interpreted *a posteriori* as the sound speed squared, and denoted by c^2. Consequently, the perturbation in pressure and density are related by the simple linear equation,

$$\delta p = c^2\delta\rho$$

It is customary to express the equations of linear acoustics in pressure rather than density. Dropping deltas in the notation, we obtain,

$$\begin{cases} c^{-2}p_{,t} & +\rho_0 v_{j,j} & = 0 \\ \rho_0 v_{i,t} & +p_{,i} & = 0 \end{cases}$$

In this report, we shall consider only time-harmonic problems. Assuming ansatz,

$$p(t,\boldsymbol{x}) = e^{i\omega t}p(\boldsymbol{x}), \quad u_i(t,\boldsymbol{x}) = e^{i\omega t}u_i(\boldsymbol{x})\,,$$

we reduce the acoustics equations to,

$$\begin{cases} c^{-2}i\omega p & +\rho_0 v_{j,j} & = 0 \\ \rho_0 i\omega v_i & +p_{,i} & = 0 \end{cases}$$

or in the operator form,

$$\begin{cases} c^{-2}i\omega p & +\rho_0\boldsymbol{\nabla}\cdot\boldsymbol{v} & = 0 \\ \rho_0 i\omega v_i & +\boldsymbol{\nabla}p & = 0 \end{cases} \tag{A.1}$$

[2]The entropy is assumed to be constant throughout the whole domain

Eliminating the velocity, we obtain the Helmholtz equation for the pressure,

$$-\Delta p - k^2 p = 0\,,$$

with the wave number $k = \omega/c$.

Having obtained the second order problem, we can proceed now with the derivation of the weak formulation, as it is usually done in most of text books on the subject. It is a little more iluminating to obtain the same variational formulation starting with the first order system. First of all, we make a clear choice in a way we treat the two equations. The equation of continuity (conservation of mass) is going to be satisfied only in the *weak sense*, i.e. we multiply it with a test function q, integrate over domain Ω and integrate the second term by parts to obtain,

$$\int_\Omega \left(\frac{i\omega}{c^2} pq - \rho_0 \boldsymbol{v} \boldsymbol{\nabla} q \right) \, d\boldsymbol{x} + \rho_0 \int_\Gamma v_n q \, dS = 0, \quad \forall q \tag{A.2}$$

Here $v_n = v_j n_j$ denotes the normal component of the velocity on the boundary.

The second equation (conservation of momentum) is satisfied in the *strong sense*, i.e. pointwise. Solving for the velocity, we get,

$$\boldsymbol{v} = -\frac{1}{\rho_0 i\omega} \boldsymbol{\nabla} p \tag{A.3}$$

In particular, the normal component of the velocity is related to the normal derivative of the pressure,

$$v_n = -\frac{1}{\rho_0 i\omega} \frac{\partial p}{\partial n}$$

At this point we introduce different boundary conditions:

- a soft boundary Γ_D,

$$p = p_0$$

- a hard boundary Γ_N,

$$v_n = v_0$$

- and an impedance condition with a constant $d > 0$,

$$v_n = dp + v_0$$

Multiplying Equation A.2 with $i\omega$, substituting the boundary data into the boundary term, and eliminating the velocity in the domain integral term, using formula A.3, we get the final variational formulation.

$$\begin{cases} p = p_0 \text{ on } \Gamma_D \\ \displaystyle\int_\Omega \left(\boldsymbol{\nabla} p \boldsymbol{\nabla} q - \left(\frac{\omega}{c}\right)^2 pq \right) \, d\boldsymbol{x} + i\omega\rho_0 d \int_{\Gamma_C} pq \, dS \;\; = -\int_{\Gamma_N \cup \Gamma_C} v_0 q \, dS \\ \qquad\qquad\qquad\qquad\qquad\qquad\qquad\qquad\qquad\qquad\qquad\qquad \forall q \;:\; q = 0 \text{ on } \Gamma_D \end{cases} \tag{A.4}$$

We have obtained the weak formulation without introducing the second order problem at all! We have a clear understanding which of the starting equations is understood in the weak, and which in a strong sense. The momentum equations, consistently with their pointwise interpretation, have been extended to the boundary to yield the appropriate boundary conditions. We mention only that all these considerations can be made more precise by introducing the language of distributions and Sobolev spaces.

AppendixA.2. Linear Elasticity

The time-harmonic linear elasticity equations include:

- balance of momentum,
$$-\rho\omega^2 u_i - \sigma_{ij,j} = f_i$$
- Cauchy displacement-strain relation,
$$\epsilon_{ij} = \frac{1}{2}(u_{i,j} + u_{j,i})$$
- consititutive law,
$$\sigma_{ij} = E_{ijkl}\epsilon_{kl}$$

The tensor of elasticities satisfies the usual symmetry assumptions,

$$E_{ijkl} = E_{jikl}, \quad E_{ijkl} = E_{ijlk}, \quad E_{ijkl} = E_{klij} \, .$$

In the case of an isotropic material,

$$E_{ijkl} = \mu(\delta_{ik}\delta_{jl} + \delta_{il}\delta_{jk}) + \lambda\delta_{ij}\delta_{kl}$$

and the constitutive law reduces to the Hooke's law,

$$\sigma_{ij} = 2\mu\epsilon_{ij} + \lambda\epsilon_{kk}\delta_{ij}$$

Utilizing the Cauchy geometric relations, we eliminate the strain tensor and represent the stresses directly in terms of the displacement gradient,

$$\sigma_{ij} = E_{ijkl}u_{k,l} \tag{A.5}$$

or, for the Hooke's law,

$$\sigma_{ij} = \mu u_{i,j} + \lambda u_{k,k}\delta_{ij} \tag{A.6}$$

The momentum equations will be satisfied in the weak sense. We multiply them with a test function v_i, integrate over Ω and integrate by parts to obtain,

$$\int_\Omega \left(\sigma_{ij}v_{i,j} - \rho\omega^2 u_i v_i\right) \, d\boldsymbol{x} - \int_\Gamma \sigma_{ij}n_j v_i \, dS = \int_\Omega f_i v_i \, d\boldsymbol{x}, \quad \forall v_i \tag{A.7}$$

We introduce now the boundary conditions,

- prescribed displacements on Γ_D,

$$u_i = u_{i,D}$$

- prescribed tractions on Γ_N,

$$t_i := \sigma_{ij} n_j = g_i$$

- prescribed impedance on Γ_C,

$$t_i + \beta_{ij} u_j = g_i$$

We restrict ourselves now to $v_i = 0$ on Γ_D, substitute the boundary data into the boundary term in Equation A.7, to obtain,

$$\int_\Omega \left(\sigma_{ij} v_{i,j} - \rho\omega^2 u_i v_i\right)\, d\boldsymbol{x} + \int_{\Gamma_C} \beta_{ij} u_j v_i \, dS = \int_\Omega f_i v_i \, d\boldsymbol{x} + \int_{\Gamma_N \cup \Gamma_C} g_i v_i \, dS \qquad \forall v_i \ : \ v_i = 0 \text{ on } \Gamma_D$$

The final variational formulation is obtained by substituting formula A.5 for stresses,

$$\left\{ \begin{array}{l} u_i = u_{i,D} \text{ on } \Gamma_D \\ \displaystyle\int_\Omega \left(E_{ijkl} u_{k,l} v_{i,j} - \rho\omega^2 u_i v_i\right)\, d\boldsymbol{x} + \int_{\Gamma_C} \beta_{ij} u_j v_i \, dS = \int_\Omega f_i v_i \, d\boldsymbol{x} + \int_{\Gamma_N \cup \Gamma_C} g_i v_i \, dS \\ \qquad\qquad\qquad\qquad\qquad\qquad\qquad\qquad\qquad\qquad \forall v_i \ : \ v_i = 0 \text{ on } \Gamma_D \end{array} \right. \tag{A.8}$$

We record the final fomulas for the bilinear and linear forms.

$$\begin{aligned} X &= \boldsymbol{H}^1(\Omega) := (H^1(\Omega))^3 \\ b(\boldsymbol{u}, \boldsymbol{v}) &= \int_\Omega \left(E_{ijkl} u_{k,l} v_{i,j} - \rho\omega^2 u_i v_i\right)\, d\boldsymbol{x} + \int_{\Gamma_C} \beta_{ij} u_j v_i \, dS \\ l(\boldsymbol{v}) &= \int_\Omega f_i v_i \, d\boldsymbol{x} + \int_{\Gamma_N \cup \Gamma_C} g_i v_i \, dS \end{aligned} \tag{A.9}$$

AppendixA.3. Elasticity Coupled with Acoustics

Let Ω be a domain in $\mathbb{R}^3$. In the following discussion we shall assume that the domain Ω is bounded. The case of an unbounded domain will be discussed in Chapter **??**. We assume that Ω is split into two disjoint parts: a subdomain Ω_e occupied by a linear elastic medium, and a subdomain Ω_a occupied by an acoustical fluid. The two subdomains are separated by an interface Γ_I. Neither the subdomains nor the interface need to be connected (they may consist of several separate pieces). The external boundary $\partial\Omega$ will be partitioned into Dirichlet, Neumann and Cauchy parts: $\Gamma_D, \Gamma_N, \Gamma_C$, respectively. Each of these boundary parts may consist of a part belonging to the boundary $\partial\Omega_e$ of the elastic subdomain, or the boundary $\partial\Omega_a$ of the acoustical subdomain. Using a more precise mathematical language, Ω_e, Ω_a are assumed to be opened and disjoint and,

$$\overline{\Omega} = \overline{\Omega}_e \cup \overline{\Omega}_a \, .$$

Similarly, elastic and acoustics parts of the Dirichlet boundary: $\Gamma_{De}, \Gamma Da$, of the Neumann boundary: $\Gamma_{Ne}, \Gamma Na$, and the Cauchy boundary: $\Gamma_{Ce}, \Gamma Ca$, are open submanifolds of $\partial\Omega$ and,

$$\partial\Omega = \overline{\Gamma}_{De} \cup \overline{\Gamma}_{Da} \cup \overline{\Gamma}_{Ne} \cup \overline{\Gamma}_{Na} \cup \overline{\Gamma}_{Ce} \cup \overline{\Gamma}_{Ca} \ ,$$

as well as,

$$\partial\Omega_e = \overline{\Gamma}_I \cup \overline{\Gamma}_{De} \cup \overline{\Gamma}_{Ne} \cup \overline{\Gamma}_{Ce} \quad \partial\Omega_a = \overline{\Gamma}_I \cup \overline{\Gamma}_{Da} \cup \overline{\Gamma}_{Na} \cup \overline{\Gamma}_{Ca} \ .$$

A two-dimensional illustration of the scenario is shown in Figure A.9.

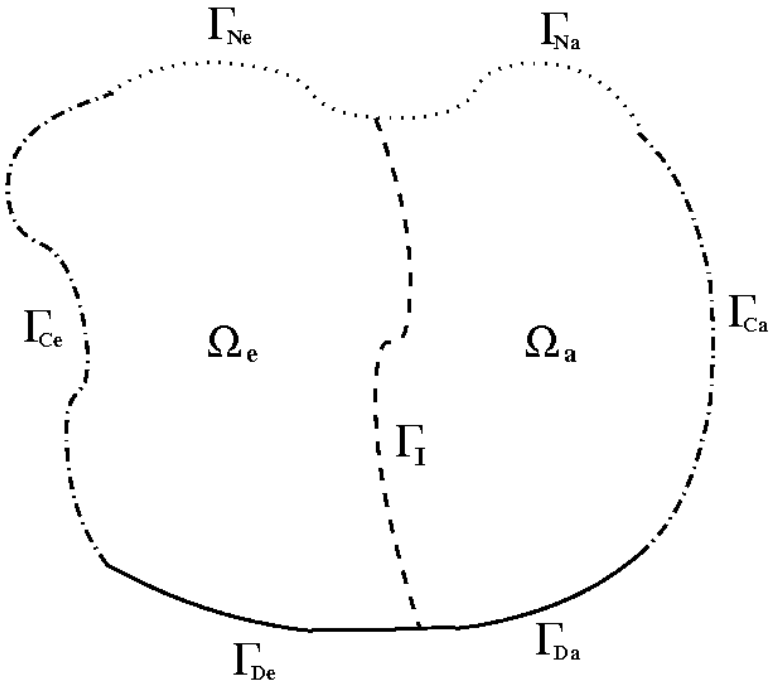

Figure A.9: Topology of a coupled problem

The coupled problem involves solving linear elasticity equations discussed in Section AppendixA.2 satisfied in subdomain Ω_e coupled with the equations of linear acoustics discussed in Section AppendixA.1 and satisfied in subdomain Ω_a. The unknowns include the components of the displacement vector $u_i(\boldsymbol{x}), \boldsymbol{x} \in \overline{\Omega}_e$ and the acoustical pressure $p(\boldsymbol{x}), \boldsymbol{x} \in \overline{\Omega}_a$. The two sets of equations are accompanied by appropriate boundary conditions and coupled by the following interface conditions:

$$i\omega u_i n_i = v_i n_i = -\frac{1}{\rho_f i\omega} \frac{\partial p}{\partial x_i} n_i, \quad t_i = \sigma_{ij} n_j = -p n_i$$

The first equation above expresses the continuity of normal component of the velocity: the normal elastic velocity has to match the normal component of the acoustical velocity. The second equation

expresses the continuity of stresses: the normal elastic stress must be equal to the (negative) pressure, whereas the tangential component of the elastic stress vector is set to zero, since the fluid does not support a shear stress. As usual, ω is the angular frequency, i is the imaginary unit, ρ_f stands for the density of the fluid, and n_i denote components of a unit vector normal to interface Γ_I which we will assume to be directed from the elastic into the acoustical subdomain. Multiplying the first interface condition by $\rho_f i\omega$, we get,

$$\rho_f \omega^2 u_n = \frac{\partial p}{\partial n}, \quad t_i = \sigma_{ij} n_j = -p n_i \tag{A.10}$$

where $u_n = u_i n_i$ denotes the normal displacement. From the mathematical point of view, the conditions of this type are classified as *weak coupling conditions*. The word "weak" refers here to the fact that the primary variable for elasticity - the displacement vector, matches the secondary variable (the flux) for the acoustic problem - the normal velocity which is related to the normal derivative of pressure. Conversely, the primary variable for the acoustic problem - the pressure, defines the flux for the elasticity problem. This "cross-coupling" is very essential in proving the well-posedness of the problem, and stability of Galerkin approximations.

On top of the interface conditions we have the usual boundary conditions for acoustics,

- prescribed pressure on Γ_{Da},
$$p = p_D$$
- prescribed normal velocity on Γ_{Na},
$$v_n = v_0$$
- an impedance condition with an impedance constant $d > 0$ on Γ_{Ca},
$$v_n = dp + v_0$$

and for the elasticity,

- prescribed displacements on Γ_{De},
$$u_i = u_{i,D}$$
- prescribed tractions on Γ_{Ne},
$$t_i := \sigma_{ij} n_j = g_i$$
- prescribed impedance on Γ_{Ce},
$$t_i + i\omega \beta_{ij} u_j = g_i$$

We proceed now with the derivation of the variational formulation. We start with the weak form of the continuity equation for acoustics,

$$\int_{\Omega_a} \left(\frac{i\omega}{c^2} pq - \rho_f \boldsymbol{v} \boldsymbol{\nabla} q \right) \, d\boldsymbol{x} + \rho_f \int_{\partial\Omega_a} v_n q \, dS = 0, \quad \forall q$$

and the weak form of the conservation of momentum for elasticity,

$$\int_{\Omega_e} \left(\sigma_{ij} v_{i,j} - \rho_s \omega^2 u_i v_i \right) \, d\boldsymbol{x} - \int_{\partial\Omega_e} \sigma_{ij} n_j v_i \, dS = \int_{\Omega_e} f_i v_i \, d\boldsymbol{x}, \quad \forall v_i$$

with ρ_s and f_i denoting the density of solid and body forces, respectively. Boundary $\partial\Omega_a$ of the acoustic subdomain is now split into the interface Γ_N and parts $\Gamma_{Da}, \Gamma_{Na}, \Gamma_{Ca}$. For the interface Γ_I, we use the first interface condition to replace the flux term $\rho_f v_n$ with $i\omega\rho_f u_n$, and proceed in the standard way with the acoustic boundary conditions, to obtain the variational statement,

$$\begin{cases} p = p_D \text{ on } \Gamma_{Da} \\ \displaystyle\int_{\Omega_a} \left(\frac{i\omega}{c^2} pq + \frac{1}{i\omega} \boldsymbol{\nabla} p \boldsymbol{\nabla} q \right) \, d\boldsymbol{x} + \int_{\Gamma_{Ca}} \rho_f d \, pq \, dS + \int_{\Gamma_I} i\omega\rho_f u_n \, q \, dS = \int_{\Gamma_{Na} \cup \Gamma_{Ca}} \rho_f v_0 q \, dS, \\ \qquad\qquad \forall q \ : q = 0 \text{ on } \Gamma_{Da} \end{cases}$$

Similarly, boundary $\partial\Omega_e$ of the elastic subdomain is split into the interface Γ_N and parts $\Gamma_{De}, \Gamma_{Ne}, \Gamma_{Ce}$. For the interface Γ_I, we use the second interface condition to replace the flux term $\sigma_{ij} n_j$ with $-pn_i$, and use the boundary conditions to obtain the variational statement,

$$\begin{cases} \boldsymbol{u} = \boldsymbol{u}_D \text{ on } \Gamma_{De} \\ \displaystyle\int_{\Omega_e} \left(E_{ijkl} u_{k,l} v_{i,j} - \rho_s \omega^2 u_i v_i \right) \, d\boldsymbol{x} + i\omega \int_{\Gamma_{Ce}} \beta_{ij} u_j v_i \, dS + \int_{\Gamma_I} p v_n \, dS = \int_{\Omega_e} f_i v_i \, d\boldsymbol{x} + \int_{\Gamma_{Ne} \cup \Gamma_{Ce}} g_i v_i \, dS, \\ \qquad\qquad \forall \boldsymbol{v} \ : \boldsymbol{v} = \boldsymbol{0} \text{ on } \Gamma_{De} \end{cases}$$

Multiplying the variational statement for acoustics by factor $i\omega$, we get the final variational formulation for the coupled problem in the form,

$$\begin{cases} \boldsymbol{u} \in \tilde{\boldsymbol{u}}_D + \boldsymbol{V}, \ p \in \tilde{p}_D + V, \\ b_{ee}(\boldsymbol{u}, \boldsymbol{v}) + b_{ae}(p, \boldsymbol{v}) = l_e(\boldsymbol{v}), \qquad \forall \boldsymbol{v} \in \boldsymbol{V} \\ b_{ea}(\boldsymbol{u}, q) + b_{aa}(p, q) = l_a(q), \qquad \forall q \in V \end{cases} \tag{A.11}$$

where:

- the bilinear and linear forms are given by the formulas:

$$\begin{aligned} b_{ee}(\boldsymbol{u},\boldsymbol{v}) = &\int_{\Omega_e} \left(E_{ijkl}u_{k,l}v_{i,j} - \rho_s\omega^2 u_i v_i\right)\, d\boldsymbol{x} + i\omega \int_{\Gamma_{Ce}} \beta_{ij}u_j v_i\, dS \\ b_{ae}(p,\boldsymbol{v}) = &\int_{\Gamma_I} p v_n\, dS \\ b_{ea}(\boldsymbol{u},q) = &-\omega^2\rho_f \int_{\Gamma_I} u_n q\, dS \\ b_{aa}(p,q) = &\int_{\Omega_a} \left(\boldsymbol{\nabla} p \boldsymbol{\nabla} q - k^2 pq\right)\, d\boldsymbol{x} + i\omega \int_{\Gamma_{Ca}} \rho_f d\, pq\, dS \\ l_e(\boldsymbol{v}) = &\int_{\Omega_e} f_i v_i\, d\boldsymbol{x} + \int_{\Gamma_{Ne}\cup\Gamma_{Ce}} g_i v_i\, dS \\ l_a(q) = &\, i\omega\rho_f \int_{\Gamma_{Na}\cup\Gamma_{Ca}} v_0 q\, dS\,, \end{aligned} \tag{A.12}$$

- $\tilde{\boldsymbol{u}}_D \in \boldsymbol{H}^1(\Omega_e) := (H^1(\Omega_e))^3$ is a finite energy lift of displacements $\boldsymbol{u}_D$ prescribed on Γ_{De}, $\tilde{p_D} \in H^1(\Omega_a)$ is a finite enery lift of pressure p_D prescribed on Γ_{Da},

- $\boldsymbol{V}$ and V are the spaces of the test functions,

$$\begin{aligned} \boldsymbol{V} &= \{\boldsymbol{v} \in \boldsymbol{H}^1(\Omega_e)\ :\ \boldsymbol{v} = \boldsymbol{0} \text{ on } \Gamma_{De}\} \\ V &= \{q \in H^1(\Omega_a)\ :\ q = 0 \text{ on } \Gamma_{Da}\} \end{aligned} \tag{A.13}$$

- $k = \omega/c$ is the acoustic wave number.

Coupled problem A.11 is symmetric if and only if diagonal forms b_{ee} and b_{aa} are symmetric and,

$$b_{ae}(p,\boldsymbol{u}) = b_{ea}(\boldsymbol{u},p)\,.$$

Thus, in order to enable the symmetry of the formulation[3], we need to rescale problem by, for instance, dividing the second equation by factor $-\omega^2\rho_f$.

[1] M. Ainsworth and J. Coyle. Hierarchic finite element bases on unstructured tetrahedral meshes. *Int. J. Num. Meth. Eng.*, 58(14):2103–2130, December 2003.

[2] L. Demkowicz. *Computing with hp Finite Elements. I.One- and Two-Dimensional Elliptic and Maxwell Problems*. Chapman & Hall/CRC Press, Taylor and Francis, October 2006.

[3] L. Demkowicz, P. Gatto, W. Qiu, and A. Joplin. $\boldsymbol{G^1}$-interpolation and geometry reconstruction for higher order finite elements. *Comput. Methods Appl. Mech. Engrg.*, 2008. published online: http://dx.doi.org/10.1016/j.cma.2008.05.026.

[3] This is essential, among other reasons, from the point of view of using a direct solver.

[4] L. Demkowicz, J. Kurtz, D. Pardo, M. Paszyński, W. Rachowicz, and A. Zdunek. *Computing with hp Finite Elements. II. Frontiers: Three-Dimensional Elliptic and Maxwell Problems with Applications*. Chapman & Hall/CRC, October 2007.

[5] L. Demkowicz, J. Kurtz, and F. Qiu. hp-adaptive finite elements for coupled multiphysics wave propagation problems. In M. Kuczma and K. Wilmański, editors, *Computer Methods in Mechanics - Lectures of the CMM 2009*. Springer Verlag, 2009. in print.

[6] W. Dong and E.S. Olson. Supporting evidence for reverse cochlear traveling waves. *J. Acoust. Soc. Am.*, pages 222–240, 2008.

[7] Böhnke F. and W. Arnold. Bone conduction in a three-dimensional model of the cochlea. *Journal of Oto-Rhino-Laryngology*, 68(6):393–396, 2006.

[8] Bekesy G. Vibration of the head in a sound field and its role in hearing by bone conduction. *The Journal of the Acoustical Society of America*, 20(6):749–760, 1948.

[9] G.N. Gatica, A. Márquez, and S. Meddahi. Analysis of the coupling of primal and dual-mixed finite element methods for a two-dimensional fluid-solid interaction problem. *SIAM J. Numer. Anal.*, 45(5):2072–2097, 2007.

[10] P. Gatto and L. Demkowicz. Construction of h1-conforming hierarchical shape functions for elements of all shapes and transfinite interpolation. Technical Report 14, ICES, 2009. Finite Elements in Analysis and Design, in review.

[11] Bleszynski M. and Bleszynski E. Mie series solution for a coupled acoustics/elasticity multalayer speher problem, 2009.

[12] A. Majda. *Compressible Fluid Flow and Systems of Conservation Laws in Several Space Variables*, volume 53 of *Applied Mathematical Sciences*. Springer-Verlag, New York, 1984.

[13] Ch. Michler, L. Demkowicz, J. Kurtz, and D. Pardo. Improving the performance of perfectly matched layers by means of hp-adaptivity. *Numer. Meth. Part. D. E.*, 2007. published online 26 April 2007 in Wiley InterScience.

[14] H.H. Nakajima, W. Dong, E.S. Olson, S.N. Merchant, M.E. Ravicz, and J.J. Rosowski. Differential intracochlear sound pressure measurements in normal human temporal bones. *Journal of the Association for Research in Otolaryngology*, 10(1):23–36, 2009.

[15] M.E. Ravicz, E.S. Olson, and J.J. Rosowski. Sound pressure distribution and energy flow within the gerbil ear canal from 100 hz to 80 khz. *J. Acoust. Soc. Am.*, 122:2154–2173, 2007.

[16] J. Schöberl. NETGEN - An advancing front 2D/3D-mesh generator based on abstract rules. *Comput.Visual.Sci*, 1:41–52, 1997. available from (http://www.hpfem.jku.at/netgen/).

[17] J. Schöberl and S. Zaglmayr. High order nédélec elements with local complete sequence property. *COMPEL: International Journal for Computation and Mathematics in Electrical and Electronic Engineering*, 24(2), 2005.

[18] W. Schroeder, K. Martin, and B. Lorensen. *The Visualization Toolkit: An Object-Oriented Approach To 3D Graphics*. Kitware, Inc., 4th edition edition.

[19] S. Stenfelt and Goode R.L. Bone-conducted sound: Physiological and clinical aspects. *Otology and Neurotology*, 2005.

[20] B.A. Szabo and I. Babuška. *Finite Element Analysis*. Wiley, New York, 1991.

[21] R. Tews and W. Rachowicz. Application of an automatic hp adaptive finite element method for thin-walled structures. *Comput. Methods Appl. Mech. Engrg.*, 198(21-26):1967–1984, 2009.